Passive Vibration Control and Tunable Damping of MEMS Resonators via Electrical Autoparametric Resonance

Sushruta Surappa and F. Levent Degertekin, *Senior Member, IEEE*

***Abstract*— Suppression of spurious vibrations and accurate control of mechanical damping is critical in MEMS devices to ensure optimal performance, sensitivity and reliability. Conventional control schemes such as feedback-based mechanical vibration absorbers or viscous dampers are either complex to implement at the micro scale or result in a higher sensor noise floor due to thermomechanical processes. In this paper, we present a tunable electrical autoparametric vibration control scheme that is applied to a capacitive MEMS resonator. In the proposed method, energy is transferred from the primary mechanical resonating element to a secondary electrical resonator via parametric mode coupling, thereby enabling dramatic reduction in the amplitude of mechanical vibration without introducing significant linear damping. As the threshold for parametric coupling is determined by electrical resistance, the system can be tuned easily to adjust the magnitude, rate and bandwidth of vibration suppression in the mechanical structure. A 1D lumped parameter model is developed to numerically analyse the behavior of the autoparametric vibration control system followed by experiments performed using a micromachined resonator array to validate the proposed model. The proposed circuit-based scheme provides an easily integratable and tunable solution to control damping in MEMS sensors and actuators. [2021-0095]**

***Index Terms*— Parametric resonance, CMUT, capacitive transducer, autoparametric vibration absorber, nonlinear dynamics.**

I. Introduction

INVESTIGATION of vibration control and damping in microelectromechanical systems (MEMS) is critical to realize increased reliability and performance in sensors and actuators. Various MEMS devices such as resonant sensors, gyroscopes and accelerometers are used to measure very small forces and displacement with high resolution and sensitivity [1]. In order to obtain optimal performance, it is necessary to isolate the MEMS from mechanical shock and unwanted ambient vibrations. Other devices like MEMS microphones are required to operate with a flat response over a wide frequency band- this requires careful control of mechanical damping in the structure in order to minimize additional sensor noise. To this effect, various active and passive vibration control and damping schemes have been proposed for MEMS devices.

A popular approach to vibration control in MEMS involves the use of active feedback mechanisms to regulate the amplitude of vibration of the structure. One such feedback mechanism makes use of piezoelectric actuators attached to the vibrating structure as part of a force feedback control loop [2]–[5]. The actuator can be utilized to enhance the Q-factor or suppress unwanted vibrations in the target structure. Active feedback can be implemented in a simpler manner in capacitive MEMS structures, as electrostatic force feedback can directly be used as a control scheme, negating the need for additional piezoelectric materials [6]–[8]. Despite the high degree of control offered by active feedback, the implementation of such mechanisms is usually complex in nature and lead to a significant increase in power consumption [9].

Alternately, various passive control schemes can provide both vibration isolation and increased damping in MEMS. Mechanical spring mass damper attachments that mimic macroscale dynamic vibration absorbers in operation have been used to isolate sensors from environmental vibrations and shock as well as suppressing higher order harmonics [10]–[12]. However, these micromachined vibration absorbing structures merely shift the resonance frequency of the primary structure, making the attachment effective only in a narrow frequency band. Moreover, it is almost impossible to tune the frequency of the absorber once fabricated. Viscous damping mechanisms such as squeeze film damping provide dissipation over a wider frequency band as compared to vibration absorbers and are intentionally introduced in MEMS microphones to provide a flat frequency response [13], [14]. Careful design of such viscous damping mechanisms is critical, as the dissipation occurs under all operating conditions and leads to an increase in the thermomechanical noise floor of the device, resulting in degradation in performance [15]. The use of shear-thickening fluids has been reported in literature as a way of providing adaptive damping depending on the magnitude of the disturbing force [16], however the encapsulation of the MEMS in a viscous liquid introduces its own set of packaging challenges.

More recently there has been growing interest in exploiting the inherent nonlinearities of resonators to control its vibration characteristics [17]. For example, parametric excitation has

Manuscript received May 6, 2021; revised September 23, 2021; accepted October 1, 2021. This work was supported in part by the Electrical, Communications and Cyber Systems (ECCS) Division of the National Science Foundation through NSF ECCS under Award 1936776 and in part by the National Science Foundation under Grant ECCS-1542174. Subject Editor I. Dufour. *(Corresponding author: F. Levent Degertekin.)*

Sushruta Surappa is with Canary Center, Stanford for Cancer Early Detection, Palo Alto, CA 94305 USA (e-mail: ssurappa@stanford.edu).

F. Levent Degertekin is with George W. Woodruff School of Mechanical Engineering, Georgia Institute of Technology, Atlanta, GA 30332 USA (e-mail: levent.degertekin@me.gatech.edu).

Color versions of one or more figures in this article are available at https://doi.org/10.1109/JMEMS.2021.3118000.

Digital Object Identifier 10.1109/JMEMS.2021.3118000

been employed to provide both amplification and damping in MEMS gyroscopes [18], [19] whereas internal resonance and nonlinear mode coupling mechanisms have also shown to be effective in controlling the ring down time in high-Q micromechanical resonators [20], [21]. Such nonlinear vibration control techniques provide a greater degree of tunability and a larger suppression bandwidth when compared to their linear counterparts. However, these mechanisms primarily rely on nonlinear coupling between multiple mechanical modes of the target structure and require precise engineering of the modal frequencies, thereby limiting widespread adoption.

In this paper, we propose a novel, tunable vibration suppression scheme in a MEMS resonator based on the principle of parametric resonance. Autoparametric vibration absorbers have previously been reported in macro scale structures and typically consist of a secondary mechanical resonator coupled to the primary vibrating structure with the resonance frequencies of the two structures arranged in a 1:2 ratio [22]–[24]. The vibration of the primary structure causes a variation in the stiffness or some other 'internal parameter' of the secondary resonator and when the amplitude of the primary structure exceeds a critical value, energy is transferred from the primary resonator to the secondary resonator via parametric mode coupling, resulting in the suppression of oscillations in the primary structure with a concurrent increase in the vibration amplitude of the secondary resonator. In this work, we replace the secondary mechanical resonator with an electrical RLC resonator [25], thereby eliminating the need for a secondary mechanical structure. The electrical resonance frequency and threshold for parametric resonance is determined by the electrical parameters which allows for easy tuning of the system. For displacements below the adjustable threshold, the parametric coupling is inactive and the circuit does not affect the response of the primary resonator, allowing for adaptable damping. As the damping mechanism only impacts the system around parametric resonance, the proposed system can be used to achieve tunable damping in MEMS resonators without introducing additional noise over the entire bandwidth as in the case of viscous damping mechanisms.

The paper is organised as follows: We first present the principle of operation of this novel approach for a capacitive MEMS resonator through a mathematical model describing the interaction between the two coupled resonators. With the help of numerical simulations, we show that the magnitude, rate and bandwidth of the suppression system can be easily controlled by adjusting the electrical parameters of the shunted circuit. The concept is then experimentally realized on a micromechanical resonator array to validate the mathematical model and demonstrate the ease of implementation of the proposed vibration control scheme with capacitive MEMS devices.

II. Principle of Operation

In the case of a capacitive MEMS resonator, the proposed autoparametric vibration absorber can be simplified and represented by a generic 1D lumped parameter model [26], [27] shown in figure 1. In this model, the mechanical resonator is represented by a parallel plate piston having an equivalent mass m, stiffness k and damping b. The resonance frequency of the piston is given by $\omega_m = \sqrt{k/m}$ and its mechanical quality factor $Q_m = \omega_m m/b$. The parallel plate piston also acts as a time-varying capacitor in the electrical domain, and is terminated with a series inductor L and resistor R to form a resonant RLC circuit having a resonance frequency $\omega_{el} = 1/\sqrt{LC_0}$, where C_0 is the static capacitance of the time-varying piston capacitor. This electrical termination enables tunable vibration control, and the combined system can be expressed in the form of the following two coupled differential equations,

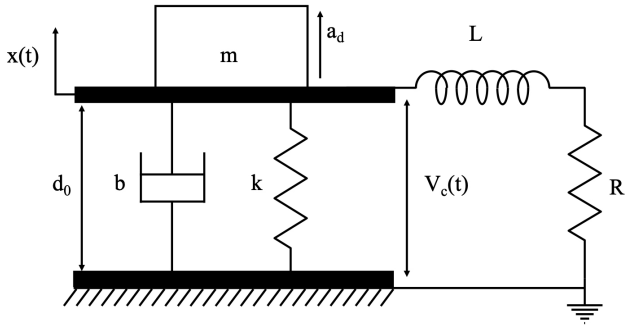

Fig. 1. 1D lumped parameter model of the mechanical resonator and the proposed electrical autoparametric absorber.

$$\left[\frac{d^2}{dt^2} + \frac{\omega_m}{Q_m}\frac{d}{dt} + {\omega_m}^2\right]x = a_d sin(\omega_d t) + \gamma\frac{V_c^2}{(d_0+x)^2} \quad (1)$$

$$\left[\frac{d^2}{dt^2} + \frac{\omega_{el}}{Q_{el}}\frac{d}{dt} + {\omega_{el}}^2(1+\frac{x}{d_0})\right]V_c = 0 \quad (2)$$

where the equation (1) mainly represents the dynamics of the mechanical resonator and equation (2) represents the electrical resonator. The harmonic acceleration applied to the resonator mass is given by a_d and its angular frequency is ω_d. V_c, x and d_0 represent the voltage across the parallel plate capacitor, the displacement of the moving plate of the capacitor and the initial vacuum gap between the plates of the capacitor respectively. The quality factor of the electrical resonator is defined as $Q_{el} = \omega_{el} L/R$.

In order to provide the conditions required for parametric coupling between the two resonators, the value of the inductor is adjusted such the electrical resonance frequency is approximately half the mechanical resonance frequency i.e., $2\omega_{el} \approx \omega_m$. Under these conditions, when the displacement of the mechanical resonator exceeds a certain threshold near its resonance frequency, it varies the capacitance of the electrical circuit at twice the electrical resonance frequency and triggers an autoparametric resonance of the electrical resonator. At this time, the electrical resonator acts as an energy sink and absorbs the vibrational energy from the mechanical resonator, thereby limiting its amplitude of motion. The drop in the mechanical motion is concurrently accompanied by a growing voltage in the electrical circuit. Most importantly, the threshold for autoparametric resonance is strongly influenced by the resistance R in the circuit, and can be tuned to provide the required

level of damping in the mechanical resonator. A thorough mathematical analysis of equations (1) and (2), leading to a quantitative description of the parametric instability tongue and the parameters affecting it is presented in [28]. When $\omega_d = 2\omega_{el}$, the minimum acceleration required to trigger autoparametric resonance is found to be,

$$a_d \geq 4\frac{\omega_m}{Q_m}\frac{\omega_{el}}{Q_{el}}d_0 \tag{3}$$

From equation (3) it can be seen that reducing R leads to an increase in Q_{el}, thereby lowering the minimum acceleration required to drive the system into parametric resonance. The upper and lower limit of the frequency band in which the system is driven into parametric resonance can also be determined for a given set of system parameters using the following expression:

$$|F| \geq \frac{4\omega^2}{\alpha}\sqrt{\gamma^2 + 4\Delta^2\omega^2}\sqrt{\beta^2 + 16\Delta^2\omega^2} \tag{4}$$

where Δ is a measure of the deviation of ω_d from $2\omega_{el}$ and F, ω, α, β and γ are normalized system parameters (see appendix A for more details). Thus by proper selection of parameters, the proposed autoparametric vibration absorber can be used as a compact, tunable and potentially completely passive solution for vibration control in capacitive MEMS resonators without the need for additional complex structures. Note that this approach is general, i.e. although the parametric coupling in the proposed system is obtained by modulating a time-varying capacitance, the same can also be achieved by modulating another variable in the electrical domain, such as the inductor as shown in [29].

III. Results

The proposed autoparametric vibration absorber is experimentally demonstrated using a micromachined capacitive resonator array. Device parameters are extracted through impedance measurements and then fitted to the numerical model to predict system performance for various mechanical and electrical operating conditions. The numerical solutions are then validated by studying the experimental device in air under ambient conditions.

A. Mechanical Resonator Design

The autoparametric vibration suppression system is analysed and demonstrated on a capacitive MEMS resonator shown in figure 2a. The resonator array measures 3.55 mm in length and 0.756 mm in width, and is fabricated using a low temperature surface micro machining process presented in [30]. The device consists of a grid of 9×34 electrostatically actuated membrane-based microresonators, with each individual membrane measuring 78 μm $\times$ 78 μm. The membranes are made by depositing a 2.2 μm thick film of low stress PECVD Si_xN_y. 200 nm thick AlSi electrodes are deposited and patterned on top of each membrane and are interconnected in a parallel configuration to enable simultaneous driving of all 306 membrane resonators. A 400 nm thick layer of chromium underneath the resonators serves as the common bottom electrode required for electrostatic actuation. The membranes and

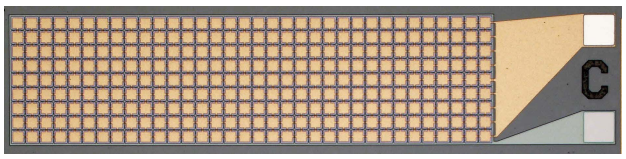

(a)

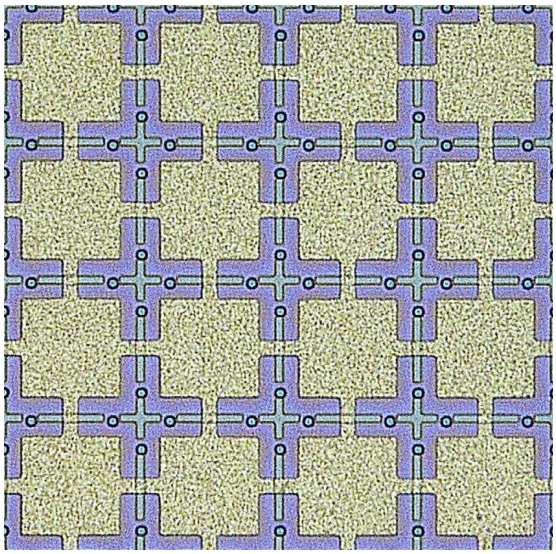

(b)

Fig. 2. (a) Top view of the capacitive MEMS resonator used in the experiment. (b) Close up view of the resonator array displaying a 4×4 grid of membranes with interconnected electrodes patterned on top of each membrane.

the bottom electrode are separated by a 380 nm vacuum gap, which corresponds to full range of membrane displacement. The vacuum gap is realized by depositing a sacrificial layer of copper on top of the bottom electrode, followed by 1 μm of the Si_xN_y membrane. Etch holes are then patterned and etched at the periphery of the membranes, and used to release the sacrificial layer via wet etching. Once the membrane is released, Si_xN_y is further deposited to seal the etch holes and build the membrane to the final desired thickness. Detailed steps involved in the fabrication process is presented in [30]

The mechanical and electrical parameters of the micromachined resonator array are obtained via impedance measurements made using a vector network analyser (Agilent 8753 ES). The mechanical resonance frequency of the resonator array is measured to be 3.8 MHz in air. The mechanical Q-factor is estimated from the bandwidth of the resonance peak and is found to be roughly 105 and the static capacitance of the array is measured to be 32 pF. These parameters are used to fully model the absorber system used in the numerical simulations and select the appropriate values of electrical components to use in the experiment.

B. Numerical Results

The 1D model of the proposed resonator-absorber system, described by equation (1) and (2), is solved in MATLAB with the ode45 solver using the system parameter values shown in

TABLE I
LIST OF PARAMETERS USED FOR THE NUMERICAL SIMULATIONS

Parameter	Value
ω_m	2πx3.8x10^6 Hz
ω_{el}	2πx1.9x10^6 Hz
Q_m	105
Q_{el}	50
γ	9.464x10^{-10} F-m/Kg
d_0	380x10^{-9} m
a_c	2πx3.8x10^6x0.012 m/s^2

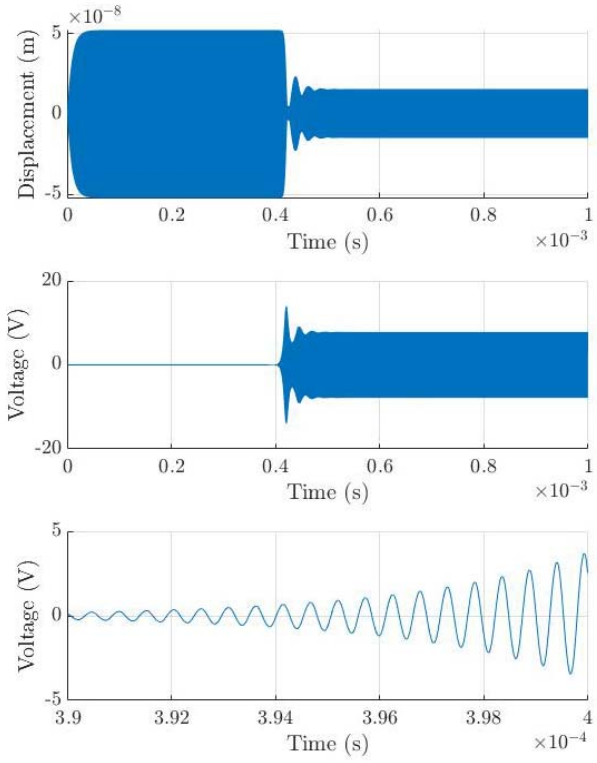

Fig. 3. Numerical simulation of displacement suppression x and autoparametric voltage build-up across the capacitor V_c using the parameters given in table I. Vibrational energy from the mechanical resonator is irreversibly transferred to the electrical resonator leading to diminishing mechanical oscillation. The third panel shows the zoomed view of the exponential voltage build up between 0.39 ms and 0.4 ms.

table I (fitted to the experimental device). The primary aim of the numerical simulations is to explore the degree of control and vibration suppression provided by the proposed scheme under different operating conditions.

The simulated response of both the mechanical resonator and the vibration suppression circuit, when a harmonic excitation above the parametric forcing threshold is applied to mechanical structure, is shown in figure 3. It is observed that initially, the displacement of the mechanical resonator increases and reaches a steady state value due to direct resonance. However during this time, energy is simultaneously transferred from the mechanical to the electrical resonator via parametric mode coupling. The rate of this energy transfer is proportional to the energy stored in the electrical mode, hence at approximately 0.4 ms, we observe a significant increase in the voltage measured across the variable capacitor accompanied by a concurrent reduction in the amplitude of mechanical resonator. The initial voltage condition provided for this particular simulation at $t = 0$ is intentionally made very small in order to slow down the rate of energy transfer and clearly observe the exchange between the oscillators. For this reason, the non-zero voltage across the capacitor at $t < 0.4$ ms is significantly smaller than the steady state value obtained after 0.4 ms and hence cannot be observed in the figure. Note that the angular frequency of the current in the circuit is exactly half the resonator drive frequency ie. $2\omega_i{=}\omega_d$.

The frequency response of the resonator to increasing excitation is shown in figure 4a. The solid lines indicate the linear response when subjected to 3 different excitation levels, in the absence of the suppression circuit. As expected, the largest excitation results in the maximum displacement response. However, in the presence of the absorber, the steady state displacement is independent of the input forcing and the displacements converge to approximately the same value for all three excitation levels (dashed lines). There is a clear, observable threshold at which parametric mode coupling is activated and the displacement starts to reduce, with the minimum steady state displacement observed close to $2\omega_{el}$.The parametric forcing threshold increases away from $2\omega_{el}$, and this is consistent with behaviour observed in parametrically excited systems [31]. Note that in the regions where the absorber is inactive, the displacement response of the resonator matches the linear case (without the absorber), indicating that the effect of the absorber is limited to the region of parametric resonance.

A major advantage with a circuit based autoparametric absorber is that it provides a means to easily tune the degree of suppression in the mechanical resonator. The minimum displacement in the resonator required for parametric coupling is strongly dependent on the electrical resistance present in the circuit. This is shown in figure 4b, where the frequency response of the mechanical resonator for a fixed level of excitation is plotted for different values of Q_{el}. It is observed that as the resistance is increased (equivalent to a reduction in Q_{el}), the resonator displacement required for parametric mode coupling also increases. Furthermore, the level of suppression provided by the absorber circuit is also reduced. For instance, when $Q_{el}{=}100$, parametric resonance takes effect when the resonator displacement exceeds 27 nm and reduces the steady state amplitude to approximately 8 nm at 3.8 MHz. In contrast, for the $Q_{el}{=}10$ case, suppression starts when the displacement exceeds 77 nm and maintains a flat frequency response in the band where it is active. Therefore, by merely adjusting the value of resistance present in the electrical circuit, it is possible to provide different levels of damping or suppression in a passive manner.

It is sometimes possible that due to manufacturing/tolerance defects or thermal drift, the electrical resonance frequency ω_{el} is not exactly one half of the mechanical resonance frequency ω_m. The performance of the vibration suppression system under such circumstances is analysed in figure 4c. It can be observed that even in the event of a slight drift

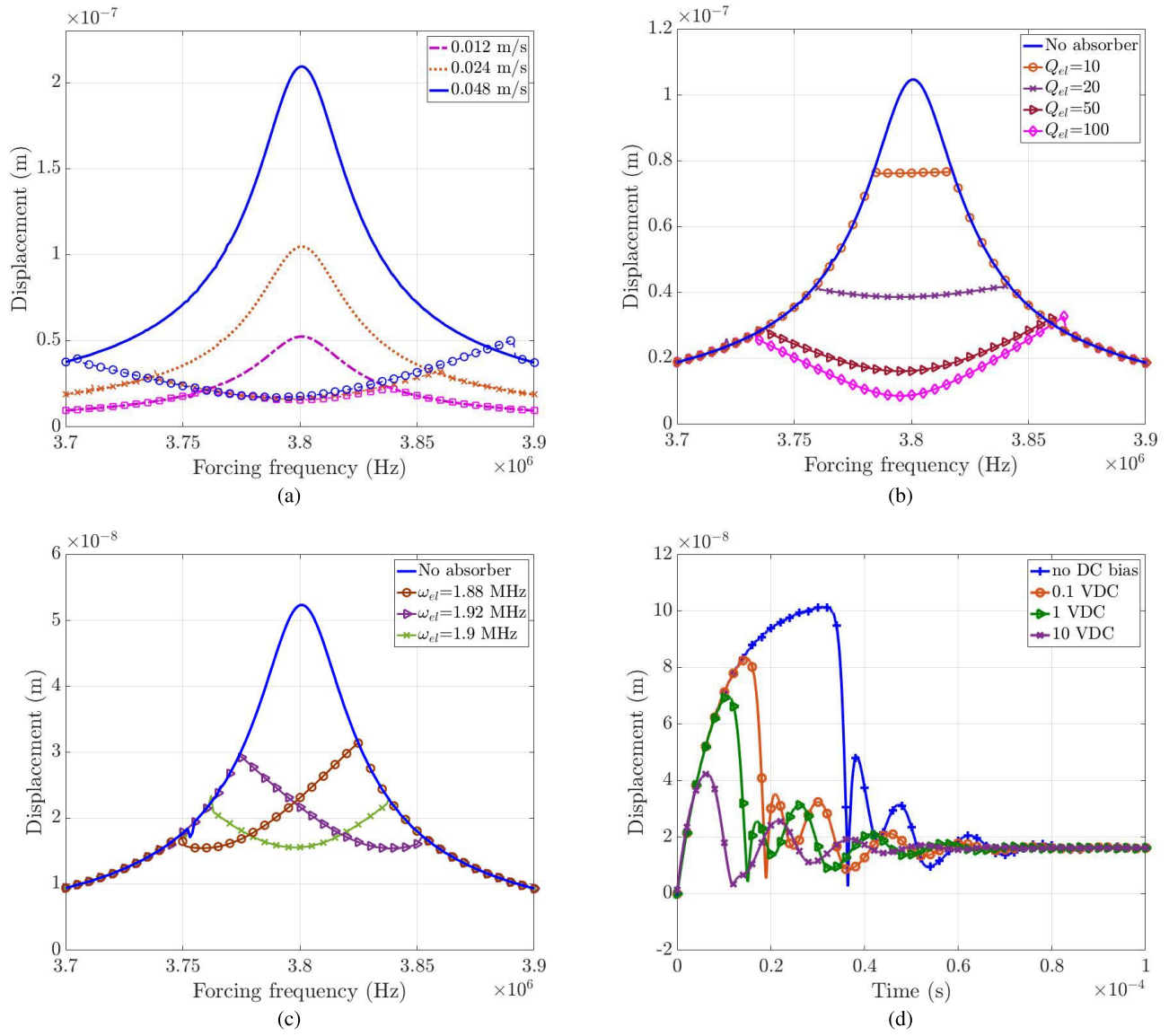

Fig. 4. Numerically simulated resonator response as a function of various system parameters. Note that unless mentioned otherwise, the parameters used are those listed in table I. (a) Frequency response of the resonator to different levels of input forcing. The electrical absorber ensures that the suppressed mechanical oscillation remains nearly the same irrespective of the exciting force. (b) The displacement threshold for autoparametric resonance increases with decreasing electrical Q-factor, thereby enabling force dependent suppression. (c) Effect of mistuned electrical resonance frequency on the effectiveness of the absorber. (d) The application of a bias voltage across the resonator results in a reduced displacement suppression time for the same input excitation of 0.024 m/s. Note that the level of suppression achieved is not affected by changing the initial bias condition.

in ω_{el}, the circuit is still capable of effectively suppressing excessive displacements in the mechanical resonator. However, the frequency at which maximum suppression occurs tends to skew heavily toward either the left or the right, depending on whether $2\omega_{el}$ is less than or greater than ω_m. Note that tuning of the electrical resonance can be achieved by changing the inductor value to match the vibration suppression frequency.

Finally, we simulate the effect of different initial conditions on the temporal response of the mechanical resonator. It can be seen from figure 4d that in the case of a fully passive autoparametric vibration absorber (thermal noise in the circuit provides the initial conditions necessary for parametric coupling), the amplitude of the mechanical resonator reaches close to its maximum steady state value before the absorber becomes active and reduces its motion. This might be undesirable in applications where rapid mechanical suppression is required to prevent catastrophic failure. In such instances, it is observed that applying a DC bias or pre-charge across the capacitive resonator can significantly reduce the time taken for mechanical suppression. A reduced suppression time also ensures that the resonator displacement does not greatly exceed the threshold at which the absorber is activated. For example, applying even a 1V DC bias causes the suppression time to reduce by more than 50% and limits the peak mechanical displacement to 70% of its maximum value, when compared to the no bias case. Note that the electrical resonance frequency is 1.9 MHz and $Q_{el} = 50$ for this simulation. Further reduction in amplitude

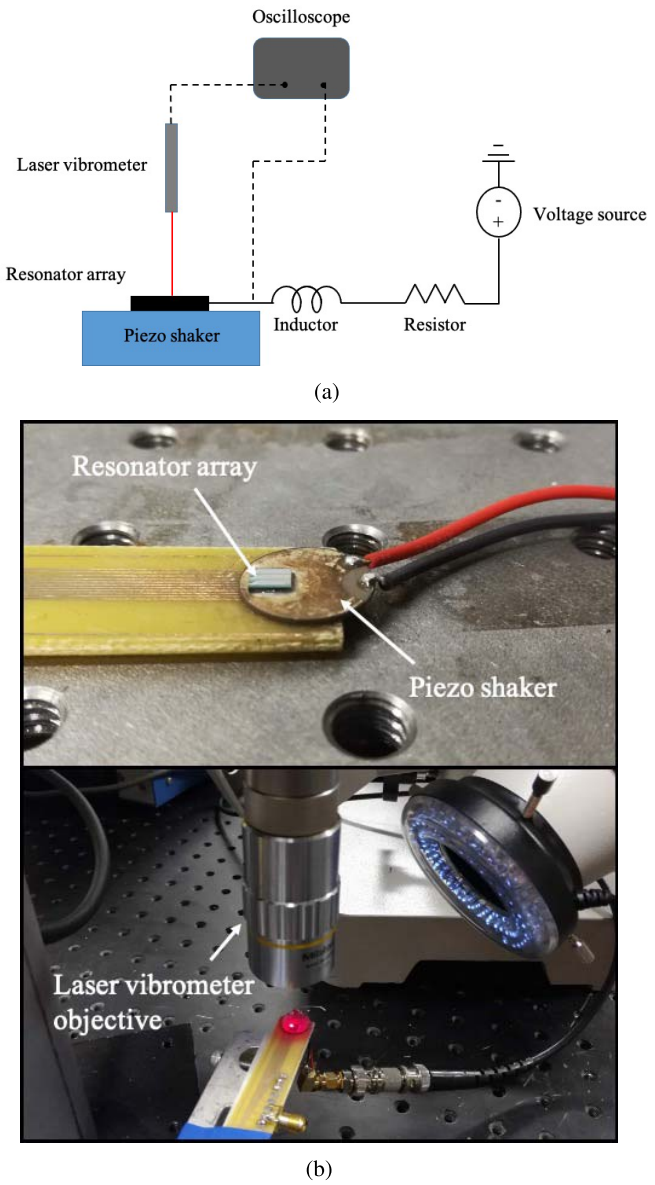

Fig. 5. (a) Schematic of the experimental setup (b) Actual experimental setup showing the mounting of the resonator on the piezo shaker as well as the vibrometer laser focused on the MEMS resonator.

and suppression time can be achieved by increasing the bias voltage. It is important to note here that it is considerably harder to control the initial conditions in purely mechanical autoparametric and internal resonance based energy transfer mechanisms whereas the implementation in this circuit based approach can be achieved by simply adding a pre-charge or battery. Note that in any practical capacitive MEMS resonator, an AC or DC bias voltage will be applied at some level for sensor readout.

These numerical results obtained by solving the coupled equations indicate that a great deal of control and flexibility can be achieved by employing a electrical autoparametric vibration suppression scheme in MEMS resonators. Vibration suppression is observed to be effective over a range of forcing excitations and the threshold and level of suppression can be controlled by tuning the electrical Q-factor. Moreover, the

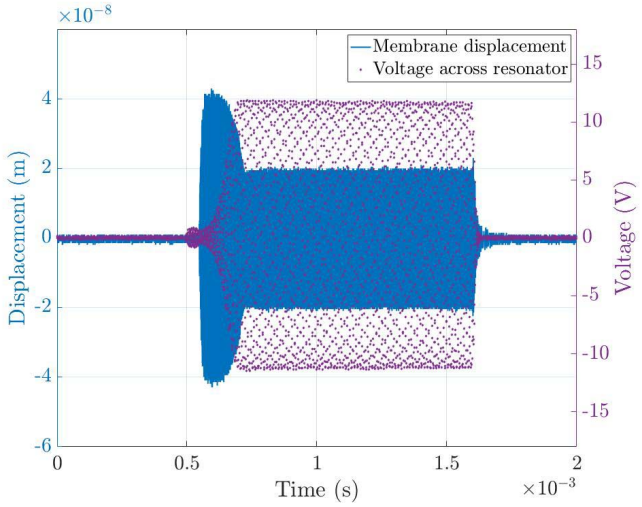

Fig. 6. Experimentally obtained time response of the membrane displacement and voltage across the resonator array. The piezo shaker is driven at 3.795 MHz and the frequency of the recorded voltage is found to be 1.9875 MHz.

ability to control the rate of suppression is an advantage when compared to purely mechanical damping techniques, making it an attractive option in high resolution MEMS sensors.

C. Experimental Results

To demonstrate the autoparametric vibration controller and validate the mathematical model, experiments are performed using the micromechanical resonator array described in section III-A. The array is bonded to a piezoelectric disc (Steminc SMD12T06R412WL) which provides the input mechanical forcing in the form of base excitations. The top electrode of the resonator array is terminated with a series 220 μH inductor and variable resistor, to form the autoparametric vibration suppression circuit. A signal generator is also added to the circuit to act as a voltage source and provide different initial conditions to the absorber circuit. The schematic of the experimental setup and the actual experiment is shown in figure 5a and 5b. A 50 ns, 100 mV unipolar electrical pulse is applied from the voltage source and the voltage across the resonator is recorded with an oscilloscope (Tektronix TDS5054b) to determine the impulse response of the electrical resonator. The resonance frequency of the circuit is measured to be 1.9 MHz with a Q-factor of 41, where the parasitic resistances in the circuit is the dominant electrical loss. A laser Doppler vibrometer (Polytec OFV 5000/534) is used to determine the mechanical response of the resonator array. With the help of a 10x objective lens, the laser spot is focused on a single membrane and the displacement is read out on the oscilloscope. Note here that the maximum displacement that can be measured with the vibrometer is limited to 75 nm whereas the full range of motion of the membrane exceeds 300 nm. In order to overcome this limitation, the spot was focused on the edge of the membrane, where the range of motion is limited. Hence, the relative displacement of the membrane in the experimental results is more indicative of absorber performance than the absolute value of displacement.

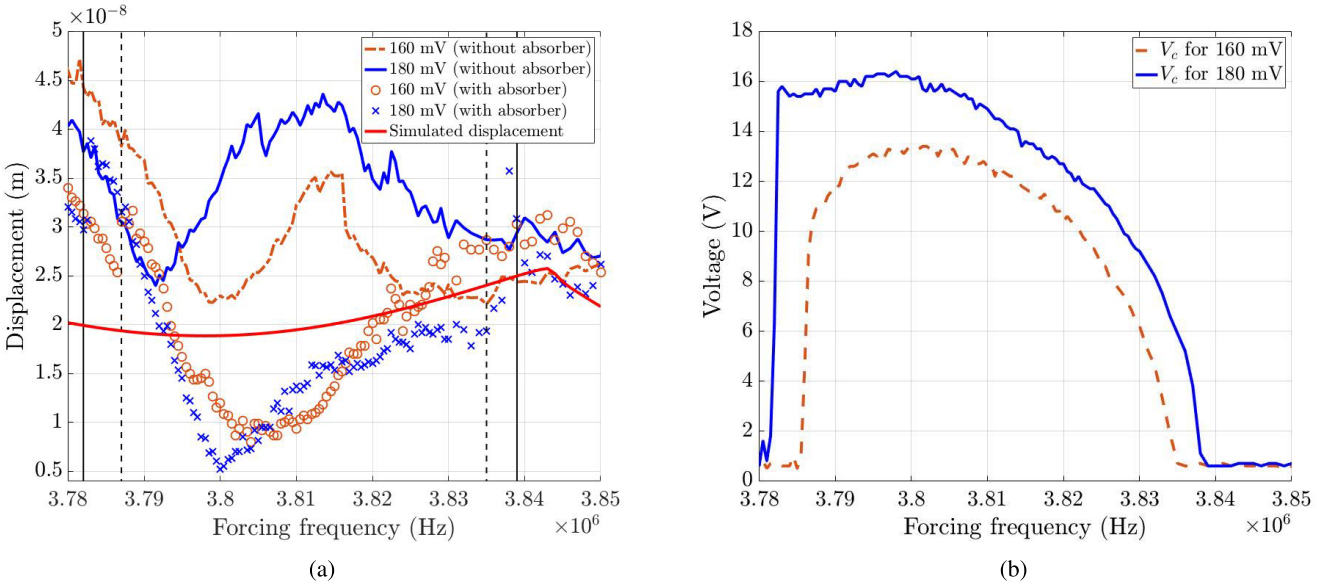

Fig. 7. (a) Experimental frequency response of resonator membrane displacement with and without the absorber. The dashed and solid vertical black lines indicate the start and end of the region of parametric resonance for 160 mV and 180 mV respectively. (b) Voltage measured across the resonator with the absorber attached. The sudden jump in voltage on the left side of the curve indicates the transition into a region of parametric resonance.

Also, the variable resistor is set to 0 Ω unless mentioned otherwise- this is because the parasitic resistances in the mechanical resonator and circuit, ranging anywhere between 25 Ω to 60 Ω, contribute to significant electrical loading.

The temporal response of a single membrane on the resonator when driven by the piezo shaker at 3.795 MHz is shown in figure 6. The input excitation from the piezo is adjusted such that there is sufficient displacement in the membrane to trigger the absorber. The voltage measured across the resonator is also overlayed in order to compare the reduction in displacement with the onset of parametric resonance. As predicted by the simulations, the reduction in membrane displacement is accompanied by a sharp increase in voltage across the resonator, with the displacement reducing to approximately 50% of its peak value. In this experiment, no external voltage is applied to the circuit. Therefore, the initial voltage conditions required for the onset of parametric resonance is provided entirely by the electromagnetic coupling and noise in the circuit, demonstrating the totally passive nature of the vibration control scheme.

A frequency sweep is performed to obtain the membrane response for two different levels of input excitation to the piezo shaker (figure 7a). As expected, the linear response of the membrane increases with higher forcing in the absence of the absorber circuit whereas the resonant response of the membrane for the same level of forcing is significantly suppressed in the presence of the circuit. Close to a 90% reduction in amplitude is observed in the presence of the absorber for the 180 mV input to the piezo shaker. The voltage that is autoparametrically built up across the resonator is also plotted in figure 7b and it can be seen that parametric resonance is triggered in the electrical circuit by a sudden jump in voltage at 3.785 MHz and 3.781 MHz for the lower and higher input excitations respectively. As the frequency is increased, the displacement of the membrane reduces to a minimum, followed by a subsequent increase until the parametric coupling between the resonators ceases. The minimum suppressed displacement also closely coincides with the center of the parametric instability region ($\omega_d \approx$3.805 Mhz). The simulated numerical frequency response of the resonator using the experimentally obtained parameters is also overlayed in figure 7a. It is clear that, qualitatively speaking, the simulated response mimics the experimental result in terms of displaying a reduced vibration amplitude in the region of parametric resonance. However there exists some deviation in terms of absolute values of displacement. This mismatch between the experimental and simulated displacement can be attributed to the fact that the simplistic 1D model does not consider the complex dynamic interactions between different membranes in the resonator array. Furthermore, parasitic capacitance and resistance, manufacturing related non-uniformities, a non-uniform resonant frequency response of the piezoelectric disc and the vibrometer range limitations prevent precise quantitative matching of the experimental and numerical results at this time.

The effect of the electrical resistance on the level of vibration suppression is presented in figure 8 for two different values of resistance. As mentioned before, in the R=0 Ω case, the electrical resistance in the circuit is purely comprised of the parasitic resistance in the microresonator, inductor and other components used to build the circuit. Ideally, minimizing these parasitic resistances allows for a greater degree of displacement suppression. The variable resistor is then adjusted to increase the resistance by 10 Ω, which causes a 14 nm increase in the minimum displacement of the membrane. This is consistent with the trends observed in the numerical simulation, where an increased resistance leads to a reduction in suppression. Further increasing the variable resistance beyond 10 Ω causes the parametric initiation threshold to exceed practically achievable levels. Hence it is critical that the system is designed with minimum parasitic resistance such that a

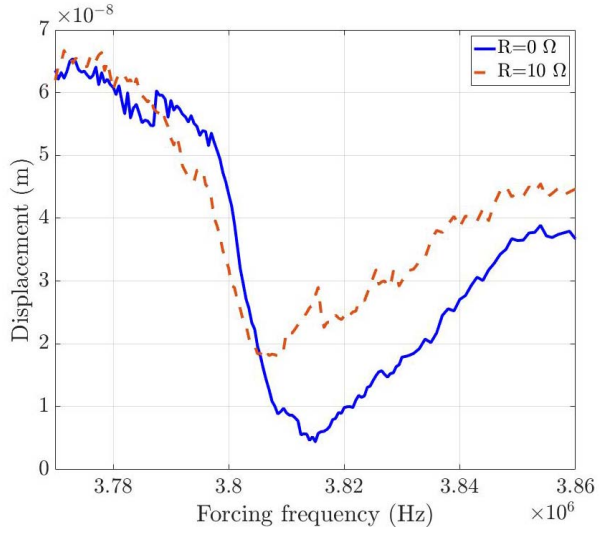

Fig. 8. Effect of varying load resistance on the experimental frequency response of the mechanical resonator.

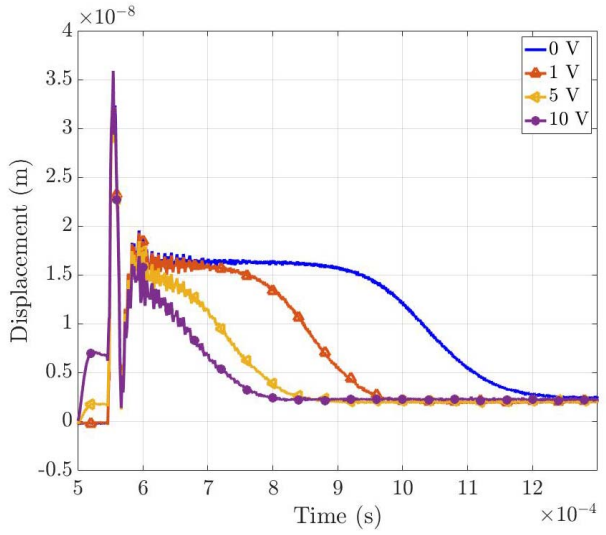

Fig. 9. Experimental envelope of membrane displacement vs. time for different initial conditions.

larger range of control can be achieved by tuning an external variable resistance.

Finally we revisit the effect of initial conditions on the response time. The envelope of the displacement response of the membrane vs. time is plotted for four different initial conditions in figure 9. To avoid unwanted effects such as spring softening on the dynamics of the resonator, a sinusoidal AC burst comprising of 60 cycles is applied from the signal generator instead of a constant DC voltage. The mechanical excitation from the piezo shaker is adjusted such that it begins just as the electrical tone burst from the generator ends. From figure 9 it can be seen that there is a large initial transient at 0.55 ms before the steady state membrane response at 3.8 MHz. This initial transient is due to the excitation of a spurious resonance very close to the membrane resonance. Such spurious resonances commonly occur in large array based resonators and are well documented in literature [32]. In this particular case, the resonance falls outside the frequency band of parametric resonance and is hence not suppressed. The steady state response of the membrane with the 10V initial condition is then parametrically suppressed within 1/6th of the time taken in the absence of any DC bias, leading to a dramatic improvement in suppression time.

Thus, these experimental results obtained by connecting an inductor and variable resistor to a capacitive micromachined resonator array validate the numerical simulations performed using the 1D lumped parameter model, despite some deviations in behaviour due to array effects such as substrate coupling, membrane cross-talk and manufacturing non-uniformities.

IV. Discussion and Conclusion

This paper presents the potential of electrical autoparametric resonance for vibration control and damping in MEMS resonators. The autoparametric absorber can be easily integrated with a MEMS device in the form of a shunted electrical circuit, and provides superior tuning capability when compared to other passive vibration control techniques. Note that this is a totally passive method when used with a regular wirewound inductor. However to have more design flexibility in terms of size and practical implementation, one can use active inductor implementation using already available power sources for the MEMS sensor. For instance, capacitive microphones or comb-drive based accelerometers introduce precisely controlled viscous damping to achieve a flat frequency response across the operational bandwidth. The proposed absorber circuit can instead be integrated with the MEMS to electrically tune the mechanical response of the resonating structure and obtain a flat frequency response without introducing additional noise over the entire bandwidth due to viscous damping. As almost all practical capacitive MEMS resonators make use of an AC or DC bias voltage for sensor readout, the wirewound inductor could potentially be replaced by synthetic op-amp based inductive elements for simpler electronics integration and smaller device footprint.

While the simulations and experiments described in this paper make use a parallel plate capacitive structure, the principle of autoparametric vibration suppression is more general and can be realized in a comb-drive electrostatic transducer or any other structure offering a time-varying capacitance. The numerical results presented in section 3B can be used as a guide to tune the appropriate electrical parameters in order to achieve the desired mechanical frequency response and rate of vibration control. Similarly, equation (3) can be used to determine the minimum electrical Q-factor required for autoparametric resonance based on both, the physical properties of the mechanical resonator, as well as the minimum acceleration acting on the MEMS. Hence through an iterative process, the autoparametric vibration absorber can be designed for optimal performance for a variety of resonator structures and applications.

In conclusion, a passive vibration control scheme is proposed in which energy is transferred from the primary resonating structure to the secondary electrical resonator via

parametric coupling, leading to a reduction in the amplitude of mechanical oscillation. The degree of suppression achievable is directly related to the Q-factor of the electrical resonator, which can be increased by reducing the resistive loss. The rate of suppression can also be controlled by introducing initial voltage conditions in the circuit. Numerical results obtained by simulating a 1D lumped model are validated by experiments performed using a micromachined capacitor array and a shunted inductor and variable resistor. The use of the absorber circuit resulted in a 90% reduction in oscillation amplitude when compared to that without the circuit. The energy transferred to the electrical resonator could also potentially be harvested, rectified and used to power nearby low power sensors. Future work will address the implementation of electrical absorbers over multiple frequency bands and explore the use of tunable damping control in micromachined membrane based metastructures.

Appendix A
Quantitative Description of the Parametric Instability Tongue

Accurate approximate analytical solutions quantifying the operational characteristics of the system described in this paper were derived and presented in our previous work [28]. The analytical solutions are based on the asymptotic analysis of the coupled nonlinear ODE's (equations 1 and 2).

To make employ the asymptotic analysis, it is required to introduce the following normalized parameters:

$$\epsilon = \frac{\mu^3 \varepsilon_0 A}{2m\zeta^2},\ \gamma = \frac{R}{L\zeta\epsilon},\ \alpha = \frac{1}{LA\varepsilon_0\zeta^2\mu\epsilon},$$
$$\beta = \frac{b}{m\zeta\epsilon},\ F = \frac{\mu F_0}{m\zeta^2\epsilon},\ D = \mu d_0,\ \omega = \frac{\omega_{el}}{\zeta}$$

where $\zeta = 10^7$ and $\mu = 10^8$. Note that A, ε_0 and F_0 refer to the area of the parallel plate piston, the free space permittivity and the force acting on the mass m due to acceleration a_d respectively. Other parameters such as the inductance L, resistance R, mechanical damping b, gap between the parallel plates d_0 and electrical resonance frequency ω_{el} have been defined in section 2. As a result, $\epsilon \ll 1$, and the timescales in the system can be separated using a nonstandard coordinate transform to obtain a more accurate approximation based on the averaging theory [33]. Two important results derived via this technique and related to the minimum forcing threshold and frequency span of the instability tongue are presented in equations 3 and 4 respectively.

Acknowledgment

The authors would like to thank Dr. Evren Arkan for fabricating the microresonator array used in the experiments and Dr. Laurence Jacobs for providing access to the laser Doppler vibrometer. Device fabrication was performed in part at Georgia Tech Institute for Electronics and Nanotechnology, a member of the National Nanotechnology Coordinated Infrastructure (NNCI).

References

[1] C. Comi, A. Corigliano, G. Langfelder, A. Longoni, A. Tocchio, and B. Simoni, "A resonant microaccelerometer with high sensitivity operating in an oscillating circuit," *J. Microelectromech. Syst.*, vol. 19, no. 5, pp. 1140–1152, Oct. 2010.

[2] N. W. Hagood and A. von Flotow, "Damping of structural vibrations with piezoelectric materials and passive electrical networks," *J. Sound Vibrat.*, vol. 146, no. 2, pp. 243–268, Apr. 1991. [Online]. Available: http://www.sciencedirect.com/science/article/pii/0022460X91907629

[3] Y. Meyer and G. Cumunel, "Active vibration isolation with a MEMS device. Effects of nonlinearities on control efficiency," *Smart Mater. Struct.*, vol. 24, no. 8, Jun. 2015, Art. no. 085004, doi: 10.1088/0964-1726/24/8/085004.

[4] W. Zhang, G. Meng, and H. Li, "Adaptive vibration control of micro-cantilever beam with piezoelectric actuator in MEMS," *Int. J. Adv. Manuf. Technol.*, vol. 28, nos. 3–4, pp. 321–327, Mar. 2006, doi: 10.1007/s00170-004-2363-5.

[5] M. Collet, V. Walter, and P. Delobelle, "Active damping with piezoelectric MEMS devices," *Proc. SPIE*, vol. 5386, pp. 301–308, Jul. 2004.

[6] H. H. Khodaparast, H. Madinei, M. I. Friswell, and S. Adhikari, "Vibration suppression in MEMS devices using electrostatic forces," *Proc. SPIE*, vol. 9799, Apr. 2016, Art. no. 979917. [Online]. Available: https://www.spiedigitallibrary.org/conference-proceedings-of-spie/9799/%979917/Vibration-suppression-in-MEMS-devices-using-electrostatic-forces/10.111% 7/12.2222069.short

[7] C. Li, H. Yang, R. N. Dean, and G. T. Flowers, "Active vibration isolator based on micromachined electrostatic actuators," *Micro Nano Lett.*, vol. 11, no. 11, pp. 715–718, Nov. 2016, doi: 10.1049/mnl.2016.0173.

[8] W. Zhou *et al.*, "Improving the dynamic performance of capacitive micro-accelerometer through electrical damping," *Microsyst. Technol.*, vol. 22, no. 12, pp. 2961–2969, Dec. 2016, doi: 10.1007/s00542-015-2694-1.

[9] M. C. Brennan and A.-M. R. McGowan, "Piezoelectric power requirements for active vibration control," *Proc. SPIE*, vol. 3039, pp. 660–669, Jun. 1997.

[10] S. W. Yoon, S. Lee, N. C. Perkins, and K. Najafi, "Shock-protection improvement using integrated novel shock-protection technologies," *J. Microelectromech. Syst.*, vol. 20, no. 4, pp. 1016–1031, Aug. 2011.

[11] J. R. Reid, V. M. Bright, and J. A. Kosinski, "A micromachined vibration isolation system for reducing the vibration sensitivity of surface transverse wave resonators," *IEEE Trans. Ultrason., Ferroelectr., Freq. Control*, vol. 45, no. 2, pp. 528–534, Mar. 1998.

[12] A. K. Delahunty and W. T. Pike, "Metal-armouring for shock protection of MEMS," *Sens. Actuators A, Phys.*, vol. 215, pp. 36–43, Aug. 2014. [Online]. Available: https://www.sciencedirect.com/science/article/pii/S0924424713005530

[13] M. Bao and H. Yang, "Squeeze film air damping in MEMS," *Sens. Actuators A, Phys.*, vol. 136, no. 1, pp. 3–27, 2007.

[14] S. S. Mohite, H. Kesari, V. R. Sonti, and R. Pratap, "Analytical solutions for the stiffness and damping coefficients of squeeze films in MEMS devices with perforated back plates," *J. Micromech. Microeng.*, vol. 15, no. 11, p. 2083, 2005.

[15] T. B. Gabrielson, "Mechanical-thermal noise in micromachined acoustic and vibration sensors," *IEEE Trans. Electron Devices*, vol. 40, no. 5, pp. 903–909, May 1993. [Online]. Available: http://ieeexplore.ieee.org/document/210197/

[16] S. S. Iyer, R. Vedad-Ghavami, H. Lee, M. Liger, H. P. Kavehpour, and R. N. Candler, "Nonlinear damping for vibration isolation of microsystems using shear thickening fluid," *Appl. Phys. Lett.*, vol. 102, no. 25, Jun. 2013, Art. no. 251902, doi: 10.1063/1.4812192.

[17] K. Asadi, J. Yu, and H. Cho, "Nonlinear couplings and energy transfers in micro- and nano-mechanical resonators: Intermodal coupling, internal resonance and synchronization," *Phil. Trans. Roy. Soc. A, Math., Phys. Eng. Sci.*, vol. 376, no. 2127, Aug. 2018, Art. no. 20170141, doi: 10.1098/rsta.2017.0141.

[18] M. Sharma, E. H. Sarraf, R. Baskaran, and E. Cretu, "Parametric resonance: Amplification and damping in MEMS gyroscopes," *Sens. Actuators A, Phys.*, vol. 177, pp. 79–86, Apr. 2012. [Online]. Available: https://www.sciencedirect.com/science/article/pii/S0924424711004742

[19] H. Wu, X. Zheng, Y. Lin, Z. Ma, and Z. Jin, "Linear parametric amplification/attenuation without spring hardening/softening effect in MEMS gyroscopes," in *Proc. IEEE 33rd Int. Conf. Micro Electro Mech. Syst. (MEMS)*, Jan. 2020, pp. 757–760.

[20] H. Okamoto, I. Mahboob, K. Onomitsu, and H. Yamaguchi, "Rapid switching in high-Q mechanical resonators," *Appl. Phys. Lett.*, vol. 105, no. 8, Aug. 2014, Art. no. 083114, doi: 10.1063/1.4894417.

[21] C. Chen, D. H. Zanette, D. A. Czaplewski, S. Shaw, and D. López, "Direct observation of coherent energy transfer in nonlinear micromechanical oscillators," *Nature Commun.*, vol. 8, no. 1, May 2017, Art. no. 15523. [Online]. Available: https://www.nature.com/articles/ncomms15523

[22] R. S. Haxton and A. D. S. Barr, "The autoparametric vibration absorber," *J. Eng. Ind.*, vol. 94, no. 1, pp. 119–125, Feb. 1972, doi: 10.1115/1.3428100.

[23] A. Zhang, V. Sorokin, and H. Li, "Energy harvesting using a novel autoparametric pendulum absorber-harvester," *J. Sound Vibrat.*, vol. 499, May 2021, Art. no. 116014. [Online]. Available: https://www.sciencedirect.com/science/article/pii/S0022460X21000869

[24] Z. Yan and M. R. Hajj, "Energy harvesting from an autoparametric vibration absorber," *Smart Mater. Struct.*, vol. 24, no. 11, Oct. 2015, Art. no. 115012, doi: 10.1088/0964-1726/24/11/115012.

[25] S. Surappa, S. Satir, and F. Levent Degertekin, "A capacitive ultrasonic transducer based on parametric resonance," *Appl. Phys. Lett.*, vol. 111, no. 4, Jul. 2017, Art. no. 043503, doi: 10.1063/1.4995564.

[26] D. J. Ijntema and H. A. C. Tilmans, "Static and dynamic aspects of an air-gap capacitor," *Sens. Actuators A, Phys.*, vol. 35, no. 2, pp. 121–128, Dec. 1992. [Online]. Available: https://www.sciencedirect.com/science/article/pii/0924424792801502

[27] J. M. Miller *et al.*, "Thermomechanical-noise-limited capacitive transduction of encapsulated MEM resonators," *J. Microelectromech. Syst.*, vol. 28, no. 6, pp. 965–976, Sep. 2019.

[28] S. Surappa, M. Tao, and F. L. Degertekin, "Analysis and design of capacitive parametric ultrasonic transducers for efficient ultrasonic power transfer based on a 1-D lumped model," *IEEE Trans. Ultrason., Ferroelectr., Freq. Control*, vol. 65, no. 11, pp. 2103–2112, Nov. 2018.

[29] N. B. Caldwell and M. F. Daqaq, "Exploiting the principle parametric resonance of an electric oscillator for vibratory energy harvesting," *Appl. Phys. Lett.*, vol. 110, no. 9, Feb. 2017, Art. no. 093903, doi: 10.1063/1.4977835.

[30] A. Pirouz and F. L. Degertekin, "Low temperature CMUT fabrication process with dielectric lift-off membrane support for improved reliability," *J. Micromech. Microeng.*, vol. 28, no. 8, Aug. 2018, Art. no. 085006.

[31] J. F. Rhoads, S. W. Shaw, K. L. Turner, J. Moehlis, B. E. DeMartini, and W. Zhang, "Generalized parametric resonance in electrostatically actuated microelectromechanical oscillators," *J. Sound Vibrat.*, vol. 296, nos. 4–5, pp. 797–829, Oct. 2006. [Online]. Available: http://www.sciencedirect.com/science/article/pii/S0022460X06002355

[32] M. Hochman, "Investigation of acoustic crosstalk effects in CMUT arrays," Ph.D. dissertation, Georgia Inst. Technol., Atlanta, GA, USA, 2011.

[33] J. Murdock, J. A. Sanders, and F. Verhulst, *Averaging Methods in Nonlinear Dynamical Systems* (Applied Mathematical Sciences Series), vol. 59. New York, NY, USA: Springer, 2007.

Sushruta Surappa received the B.S. degree in mechanical engineering from Visvesvaraya Technological University, India, in 2012, and the M.S. and Ph.D. degrees in mechanical engineering from Georgia Institute of Technology, GA, USA, in 2015 and 2021, respectively. As part of his Ph.D. work, he developed a new class of nonlinear MEMS transducers with applications in wireless power transfer, sensing, and energy harvesting. He is currently a Post-Doctoral Researcher with the Canary Center for Early Cancer Detection, Stanford University, where research focuses on developing various MEMS-based tools for the separation and capture of extracellular vesicles for early cancer detection. He is passionate about developing low-cost technologies for medical diagnostics and is a keen proponent of science communication.

F. Levent Degertekin (Senior Member, IEEE) received the B.S. degree from Middle East Technical University, Turkey, in 1989, the M.S. degree from Bilkent University, Turkey, in 1991, and the Ph.D. degree from Stanford University, CA, USA, in 1997, all in electrical engineering.

He worked at Edward L. Ginzton Laboratory, Stanford University, first as a Visiting Scholar from 1992 to 1993 and then as an Engineering Research Associate from 1997 to 2000. He is currently the G. W. Woodruff Chair of Mechanical Systems and a Professor with George W. Woodruff School of Mechanical Engineering and the School of Electrical and Computer Engineering, Georgia Institute of Technology, GA, USA. He has authored over 60 U.S. patents and over 140 journal publications. His research interests have been in micromachined acoustic and opto-acoustic devices, integrated systems for medical ultrasound imaging, bioanalytical instrumentation, and atomic force microscopy. He has received the NSF CAREER Award for his work on ultrasonic atomic force microscopy in 2004, the IEEE Ultrasonics, Ferroelectrics, and Frequency Control (UFFC) Society 2004 Outstanding Paper Award with his students, and the inaugural IEEE UFFC Society Carl Hellmuth Hertz Ultrasonic Achievement Award in 2014. He was an Associate Editor of the IEEE SENSORS JOURNAL and the IEEE TRANSACTIONS ON ULTRASONICS, FERROELECTRICS AND FREQUENCY CONTROL.